Vol 454|17 July 2008|doi:10.1038/nature07136

LETTERS

Generation of Fock states in a superconducting quantum circuit

Max Hofheinz[1], E. M. Weig[1]†, M. Ansmann[1], Radoslaw C. Bialczak[1], Erik Lucero[1], M. Neeley[1], A. D. O'Connell[1], H. Wang[1], John M. Martinis[1] & A. N. Cleland[1]

Spin systems and harmonic oscillators comprise two archetypes in quantum mechanics[1]. The spin-1/2 system, with two quantum energy levels, is essentially the most nonlinear system found in nature, whereas the harmonic oscillator represents the most linear, with an infinite number of evenly spaced quantum levels. A significant difference between these systems is that a two-level spin can be prepared in an arbitrary quantum state using classical excitations, whereas classical excitations applied to an oscillator generate a coherent state, nearly indistinguishable from a classical state[2]. Quantum behaviour in an oscillator is most obvious in Fock states, which are states with specific numbers of energy quanta, but such states are hard to create[3–7]. Here we demonstrate the controlled generation of multi-photon Fock states in a solid-state system. We use a superconducting phase qubit[8], which is a close approximation to a two-level spin system, coupled to a microwave resonator, which acts as a harmonic oscillator, to prepare and analyse pure Fock states with up to six photons. We contrast the Fock states with coherent states generated using classical pulses applied directly to the resonator.

The difficulty of generating quantum number states in a linear resonator has been overcome by interposing a nonlinear quantum system, such as an ion, between a classical radiation source and the resonator. A classical pulse applied to the nonlinear system creates a quantum state that can subsequently be transferred to the resonator. Repeating this process multiple times results in a quantum number state in the resonator. Such a method was used to deterministically generate Fock number states for the mechanical motion of ions in a harmonic ion trap[3]. The analogous deterministic creation of Fock states in electrodynamic resonators has only been demonstrated for states with one or two photons[5,6], although Fock states with larger photon numbers have been recorded using projective measurements[7,9]. The deterministic creation of pure Fock states in a solid-state system, as described here, represents a significant step forward. Solid-state systems permit highly complex integrated circuitry to employ such bosonic states in, for example, quantum computational architectures. The integration of microwave resonators with solid-state qubits has recently attracted much interest[10–16], but to date such implementations have only used zero or one photons in the resonator, putting the system in a regime where the bosonic nature of the linear resonator is not apparent.

The method we use here to generate multi-photon Fock states is scalable to arbitrary photon numbers[3,17], limited only by decoherence times and the speed at which photons can be transferred to the resonator. We generate the Fock states using the qubit as an intermediary between a classical microwave source and the resonator. The Fock states are compared to coherent states generated by driving the resonator directly with a classical radiation pulse. In both cases we measure the resonator state through the photon number dependence of the qubit–resonator coupling, monitored using the qubit[18]. The complexity of the pulse sequences used to create and analyse the

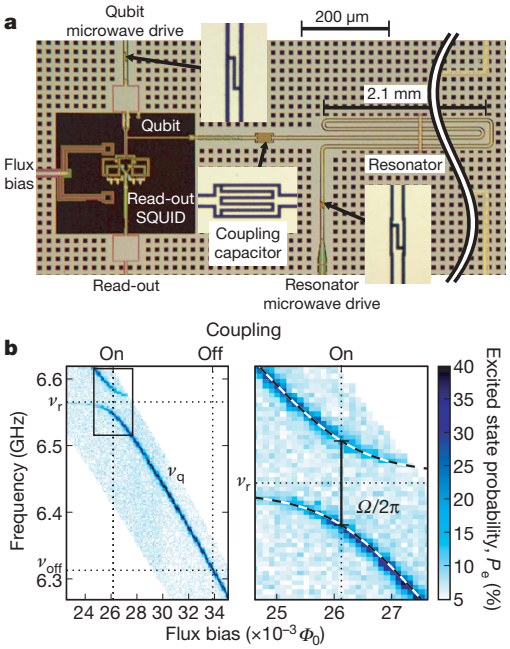

Figure 1 | Device description and spectroscopy. a, Photomicrograph of a phase qubit (left) coupled to a co-planar waveguide resonator (right). The resonator has a total length of 8.76 mm. A microwave line capacitively coupled to the qubit is used to inject individual photons into the qubit. A second capacitor between the qubit and resonator couples these two quantum systems, with the resonant interaction controlled by tuning the qubit using a flux bias. The resonator can also be directly excited using a second capacitively coupled microwave line. **b**, Spectroscopy of qubit and resonator. The false-colour images show the excited state probability P_e of the qubit as a function of driving frequency and flux bias in units of the flux quantum $\Phi_0 = h/2e$, where e is the elementary charge. A dark line is seen when the frequency of the microwave drive matches an eigenfrequency of the qubit–resonator system. An avoided crossing appears when the qubit is tuned through the resonator frequency ν_r. A detailed view of the avoided crossing is shown in the right-hand subpanel, superposed with a fit (black-and-white dashed line) to the Jaynes–Cummings model in equation (1). The fitting parameters are the magnitude of the splitting $\Omega/2\pi = 36.0 \pm 0.6$ MHz (s.e.m. uncertainty; vertical bar) and the resonator frequency $\nu_r = 6.5666 \pm 0.0005$ GHz (s.e.m. uncertainty; dotted horizontal line). The dotted vertical lines respectively indicate the qubit operating points when the qubit–resonator coupling is on and off.

[1]Department of Physics, University of California, Santa Barbara, California 93106, USA. †Present address: Ludwig-Maximilians-Universität, Geschwister-Scholl-Platz 1, 80539 München, Germany.

resonator states, and the high fidelity of the resulting measurements, demonstrate a significant advance in the control of superconducting quantum circuits.

Our experimental system (Fig. 1a) is based on the superconducting phase qubit, a device developed for quantum computation[8]. To a good approximation this qubit is represented by a two-level spin system, with ground state $|g\rangle$ and excited state $|e\rangle$. These states are separated in energy by a transition frequency ν_q that may be tuned from about 6 to 9 GHz using an external flux bias. With the application of classical microwave pulses, the quantum state of the qubit can be fully controlled[19]. The qubit state is measured by a destructive single-shot measurement, achieved by applying a flux-bias pulse to the qubit. This pulse causes the state $|e\rangle$ to tunnel to a state that can be easily distinguished from the state $|g\rangle$ with a flux measurement performed using a read-out d.c. superconducting quantum interference device (SQUID)[20]. The measurement visibility, that is, the difference between the tunnelling probabilities for states $|e\rangle$ and $|g\rangle$, is 80%. Decoherence of the qubit is characterized by measurement of the energy relaxation time $T_1^q \approx 550$ ns and phase coherence time $T_2^q \approx 100$ ns.

The qubit is coupled to a high-Q-factor superconducting co-planar waveguide resonator[21], which serves as a harmonic oscillator, with a resonance frequency $\nu_r = 6.5666 \pm 0.0005$ GHz. The coupling is achieved using a capacitor, which sets the coupling strength $\Omega/2\pi = 36.0 \pm 0.6$ MHz, measured using spectroscopy[22] (Fig. 1b). Achieving strong coupling ($\Omega \gg 1/T_1$) between a phase qubit and a resonator is straightforward[23,24], as the qubit characteristic impedance of ~30 ohms is well matched to the resonator characteristic impedance of ~50 ohms. The coupling between the qubit and the resonator can be effectively turned off by biasing the qubit well out of resonance, at a frequency $\nu_{off} = 6.314$ GHz, where the coupling is effectively reduced by a factor of $(\nu_r - \nu_{off})^2/(\Omega/2\pi)^2 \approx 50$. Microwaves can also be injected directly into the resonator through a separate microwave feed line. The decoherence times of the resonator were measured to be $T_1^r \approx 1\,\mu s$ and $T_2^r \approx 2\,\mu s \approx 2T_1^r$ (E. M. Weig *et al.*, manuscript in preparation). All measurements were performed in a dilution refrigerator operating at 25 mK, which is much less than $h\nu_r/k_B$ and $h\nu_q/k_B$ (where k_B and h are the Boltzmann and Planck constants, respectively), so thermal noise in this system is negligible.

When the qubit and resonator are tuned off resonance, such that $|\nu_r - \nu_q| \gg \Omega/2\pi$, no photons are exchanged between the qubit and resonator. On resonance, for $|\nu_r - \nu_q| \ll \Omega/2\pi$, energy can be exchanged between the two systems, and the state of the system can oscillate. The dynamics of energy exchange between the resonator and qubit can be approximated within the rotating-wave

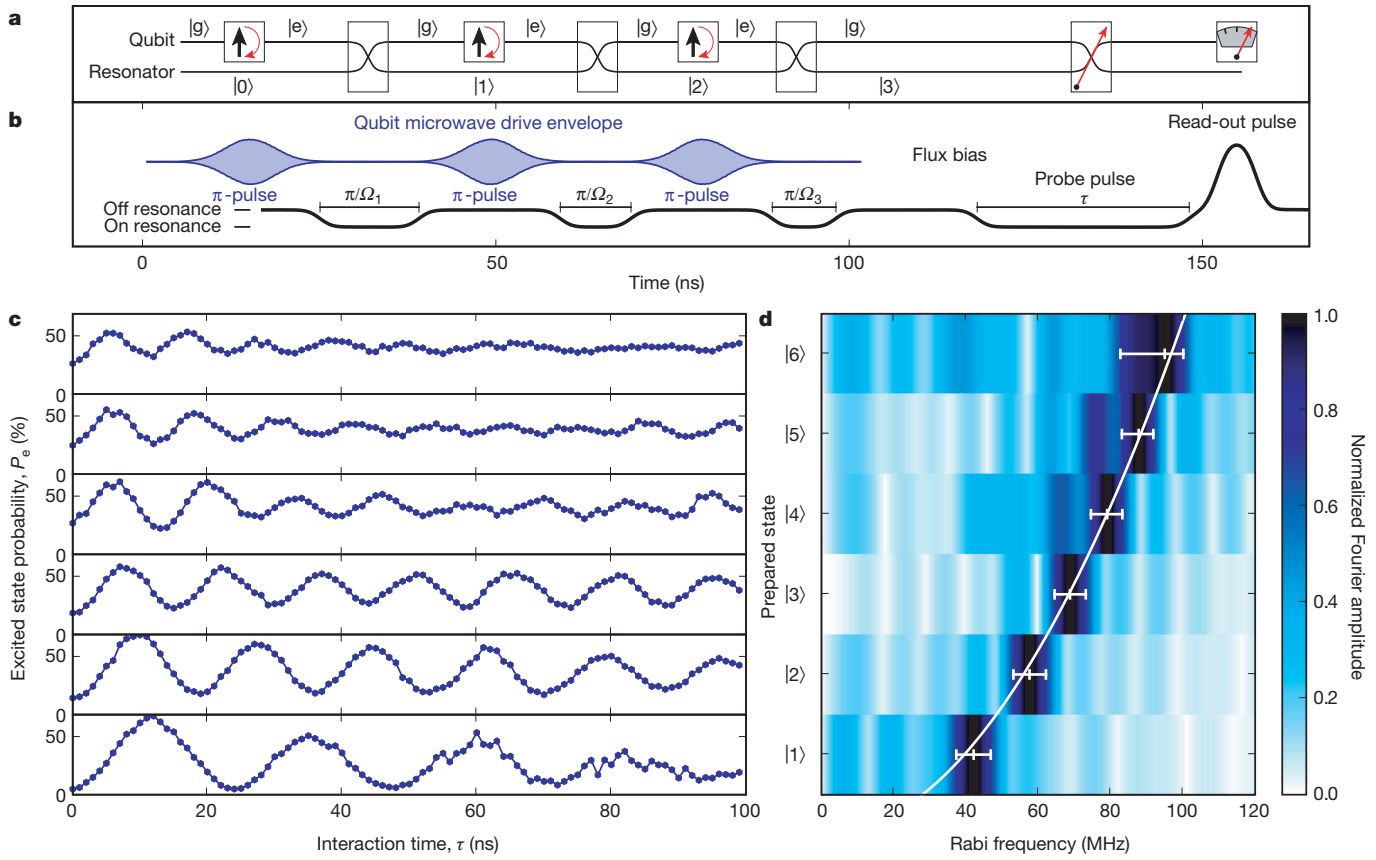

Figure 2 | Preparation and measurement of Fock states. a, Quantum program and **b**, pulse sequence for the qubit microwave signal and flux bias used to implement it. An excitation is created in the qubit with a resonant microwave pulse and then transferred to the resonator by tuning the qubit into resonance for half an oscillation period. This sequence is repeated until the desired photon number n is reached; $n = 3$ in the example depicted here. The length of the tuning pulse decreases as $1/\sqrt{n}$. To analyse the resonator state the qubit is tuned into resonance for a variable interaction time τ and the qubit state is finally read out by applying a high-flux-bias pulse that makes the excited state tunnel into a state which can be easily distinguished from the ground state. **c**, Plot of the probability of the excited qubit state P_e versus interaction time τ for Fock states with $n = 1, \ldots, 6$. The time traces show sinusoidal oscillations with a period that shortens with increasing photon number n. **d**, The false-colour image shows the Fourier amplitudes of the traces in **c**, obtained with a 100-ns rectangular window function after subtracting the average value. Each Fourier transform displays a clear peak at the n-photon oscillation frequency Ω_n, indicating the high purity of the Fock states. The peak maxima are marked, with the error bars indicating their −3-dB points. The white curve is the expected $\sqrt{n}$ scaling, adjusted to fit the data using the coupling strength $\Omega/2\pi = 40 \pm 1$ MHz (s.e.m. uncertainty), which is slightly higher than that determined from spectroscopy. In addition, the actual photon number scaling of the oscillation frequency is slightly slower than $\sqrt{n}$. Both deviations can be attributed to detuning of the qubit with respect to the resonator, as discussed in the text.

approximation by the Jaynes–Cummings model Hamiltonian[25]

$$H_{\mathrm{int}} = \frac{\hbar\Omega}{2}\left(a\sigma_+ + a^\dagger\sigma_-\right) \quad (1)$$

where $a^\dagger$ and a are respectively the photon creation and annihilation operators for the resonator, σ_+ and σ_- are respectively the qubit raising and lowering operators and $\hbar = h/2\pi$. If the system is prepared in the state $|g\rangle|n\rangle$ (qubit in the ground state, n photons in the resonator), the system will oscillate between this state and the state $|e\rangle|n-1\rangle$ at an angular frequency $\Omega_n = \sqrt{n}\,\Omega$. This $\sqrt{n}$ dependence of the oscillation frequency is the cavity quantum electrodynamic equivalent of stimulated emission: a photon is transferred between resonator and qubit more rapidly when more photons are present in the resonator. This increase in oscillation frequency is the key to our measurement of the resonator state[18].

In order to prepare the resonator in a Fock number state, we begin with the qubit detuned from the resonator and wait a time much longer than T_1^{r} or T_1^{q}, allowing both qubit and resonator to relax to their respective ground states $|g\rangle$ and $|0\rangle$. As shown in Fig. 2a, b, we then apply a gaussian microwave pulse to the qubit at $\nu_{\mathrm{q}} = \nu_{\mathrm{off}}$, with an amplitude and duration that are calibrated to yield the state $|e\rangle$. We obtain ~98% fidelity for this operation when implemented with properly shaped pulses[26]. The qubit and resonator are then tuned into resonance for a time $\pi/\Omega_1 = \pi/\Omega$ so that the excitation in the qubit is transferred to the resonator. The time and amplitude of the tuning pulse are adjusted to yield the best state transfer, determined by maximizing the probability of finding the qubit in the state $|g\rangle$ directly after the pulse. A second microwave pulse is then applied to the qubit to re-prepare it in the state $|e\rangle$. The qubit and resonator are brought back into resonance, but for a reduced time $\pi/\Omega_2 = \pi/\sqrt{2}\,\Omega$. After this procedure has been repeated n times, with an appropriate reduction in the transfer time for each successive photon, we obtain a final state $|g\rangle|n\rangle$ corresponding to an n-photon Fock state in the resonator.

To analyse the resonator state, we tune the qubit and resonator into resonance for an adjustable interaction time τ and then read out the qubit state. The probability $P_{\mathrm{e}}(\tau)$ of finding the qubit in the state $|e\rangle$ is obtained by averaging 3,000 pulse sequences for each interaction time τ. The probability is expected to oscillate in the absence of decoherence according to[2]

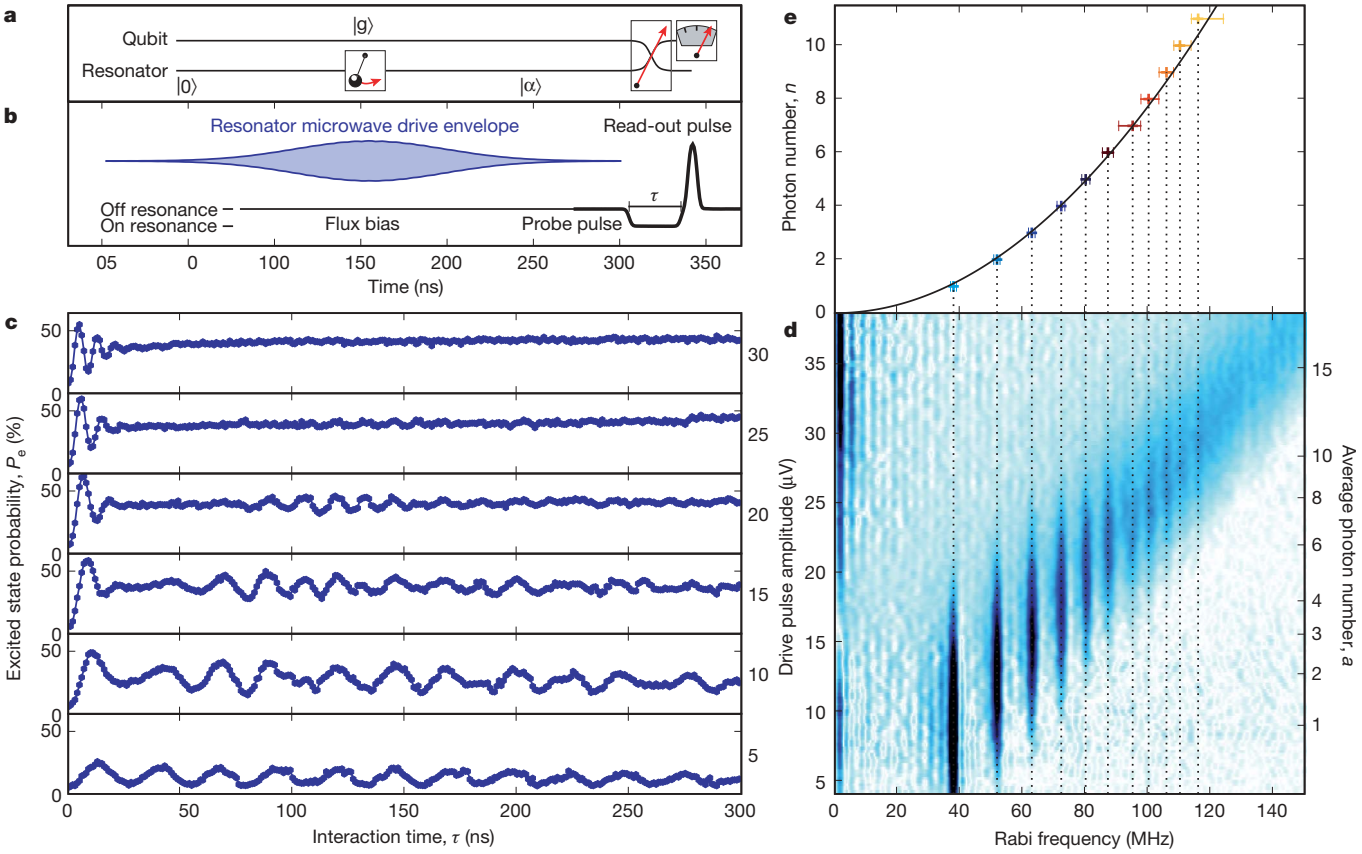

Figure 3 | Preparation and measurement of coherent states. **a**, Quantum program and **b**, pulse sequence of the resonator microwave drive and the qubit bias used to implement it. A gaussian pulse with 100-ns full-width at half-maximum and varying amplitude is directly applied to the resonator and creates a coherent state $|\alpha\rangle$. The qubit, in its ground state, is then brought into resonance for a variable interaction time τ and measured, exactly as for the Fock state measurements. **c**, Plot of the excited state probability P_{e} versus interaction time τ for six different microwave amplitudes. The time traces are aperiodic because of the irrational ratios in the oscillation times for the different photon number states $|n\rangle$ comprising the coherent state. **d**, Fourier transform of the data in **c**, obtained with a 300-ns rectangular window function after subtracting the average value. Darker colours indicate higher amplitudes. The data have been smoothed in the drive pulse direction with a $\sigma = 0.2$-μV gaussian low-pass filter. The Fourier spectrum reveals a sharp peak at each number state frequency for $n = 1, \ldots, 11$. **e**, Frequencies of the n-photon Fourier peaks compared to the expected $\sqrt{n}$ scaling, adjusted to fit the data using the coupling strength $\Omega/2\pi = 36.0 \pm 0.3$ MHz (s.e.m. uncertainty), which matches that determined from spectroscopy. As in Fig. 2d, the actual scaling is slightly slower than $\sqrt{n}$. The error bars indicate the −3-dB points of the Fourier transform peaks.

$$P_e(\tau) = \sum_{n=1}^{\infty} P_n \frac{1-\cos(\Omega_n \tau)}{2} \quad (2)$$

where P_n is the probability of initially having n photons in the resonator. For a pure Fock state $|n\rangle$, P_e oscillates at the frequency $\Omega_n/2\pi$. When several different $|n\rangle$ states are occupied, the time dependence of $P_e(\tau)$ becomes more complex, owing to the irrational ratios of the oscillation frequencies Ω_n. Note that although P_0 does not enter equation (2) directly, it is given by the time average

$$\bar{P}_e = \sum_{n=1}^{\infty} \frac{P_n}{2} = \frac{1-P_0}{2} \quad (3)$$

The experimental time dependence of $P_e(\tau)$ is displayed in Fig. 2c for Fock states with $n = 1, \ldots, 6$. The time traces are approximately sinusoidal, indicating from equation (2) that for each initial state, one photon number dominates in the resonator state. The oscillations have large amplitudes for $n = 1, 2, 3$, and gradually decrease for $n = 4, 5, 6$. Both the amplitude and the decay time decrease with increasing photon number n because the lifetime of an n-photon Fock state decreases as T_1^r/n (ref. 27) and the time needed to create such a state increases as n. For $n = 6$, the lifetime of the Fock state and the length of the preparation sequence are comparable.

The period of the oscillations clearly decreases with n. The period of the state $|4\rangle$, for example, is approximately half the period of the state $|1\rangle$, as expected from the $\sqrt{n}$ scaling of the oscillation frequency. A more quantitative analysis of this dependence is shown in Fig. 2d, where the Fourier transforms of the time traces are plotted: each displays a clear peak at a single frequency, which scales approximately as $\sqrt{n}\,\Omega/2\pi$. The actual frequency dependence is slightly slower than $\sqrt{n}$, and the coupling strength $\Omega/2\pi = 40$ MHz is slightly larger than the one obtained from the splitting in Fig. 1. Both deviations can be explained by our having used an 'on' operating point slightly detuned from the minimal splitting in Fig. 1b, yielding slightly higher oscillation frequencies. The oscillation frequencies for higher photon number states, however, are less affected by detuning because they are more strongly coupled to the qubit. Indeed, for this experiment we choose the on-point such as to maximize state transfer between the qubit and the resonator. This on-point is slightly off resonance owing to imperfections in the tuning pulses.

We next highlight the non-classical features of the Fock states by comparing them with coherent states, the quantum equivalent of classical oscillations, that are created when a harmonic oscillator is driven directly with a classical signal. To generate such states we drive the resonator with a gaussian-shaped resonant microwave pulse with a full-width at half-maximum of 100 ns (Fig. 3a, b) and a range of amplitudes. The qubit is not involved in this state preparation and stays in the ground state. The read-out of the resonator state is performed using the qubit, exactly as for the Fock state analysis.

In a coherent state the amplitude and phase of the oscillation are well defined, but the number of photons is not. A coherent state is a superposition of different Fock states for which the occupation probability P_n of an n-photon Fock state follows a Poisson distribution that depends on the average photon number a:

$$P_n(a) = \frac{a^n e^{-a}}{n!} \quad (4)$$

As a result, the time dependence of $P_e(\tau)$ (Fig. 3c) is strikingly different from that observed for the Fock states. At low drive amplitude, $P_e(\tau)$ is periodic but has low visibility because for $a \ll 1$ all P_n for $n > 1$ are vanishingly small and P_1 itself is small. At higher drive amplitudes, the time traces display a strong initial ringing with fast collapse, followed by a revival—a characteristic feature of a coherent state coupled to a two-level system[28,29]. During the revival, the time dependence is irregular because the coherent state is composed of different Fock states that oscillate with irrational frequency ratios.

The decomposition of the coherent states into Fock states becomes very clear in the Fourier transforms of the time traces (Fig. 3d). The oscillation frequencies for different photon number states appear as sharp vertical lines, indicating the underlying quantum nature of the coherent states. With increasing pulse amplitude, the lines corresponding to higher photon numbers become more pronounced, and at any given pulse amplitude there are several sequential photon number states with significant occupation probabilities. In Fig. 3e, the oscillation frequencies corresponding to the maxima of these lines are plotted versus the corresponding photon number. The dependence on photon number matches that observed previously in the analysis of the Fock states.

These data also show good quantitative agreement with the expected Poisson distributions. In Fig. 4 we plot the photon number state probabilities P_n obtained from the Fourier amplitudes along the dashed vertical lines in Fig. 3d. Their dependence on drive amplitude agrees very well with the Poisson distributions, which are plotted as solid lines. The Poisson distribution for each photon number n has been scaled by a visibility (Fig. 4 inset). The visibility for $n = 0$ is close to 100%. The visibility for higher photon number states is lower because the Fourier amplitude is reduced by decoherence during the interaction time of 300 ns. We find that shorter interaction times yield much higher visibilities, but at the cost of lower frequency resolution in Fig. 3d, e.

We note that, unlike that for a pure Fock state, the photon number distribution for a coherent state does not reveal the entire quantum description of the resonator state, because a number state analysis cannot by itself distinguish a statistical mixture from a pure coherent state. A full quantum analysis would involve a complete tomographic measurement, yielding, for example, the Wigner function[30]. Given the high fidelity of our Fock state measurements and the excellent agreement with the coherent state analysis, we believe that such an experiment should be possible in the near future.

In conclusion, we have created multi-photon Fock states for the first time in a solid-state system. The highest photon number we have achieved to date, $n = 6$, is limited only by the coherence times of the qubit and the resonator. In our experiment, the Fock states are created on demand in a completely deterministic fashion. This presents the possibility of using complex bosonic states in solid-state-based quantum algorithms, which until now have only involved spin-1/2-like (fermionic) states.

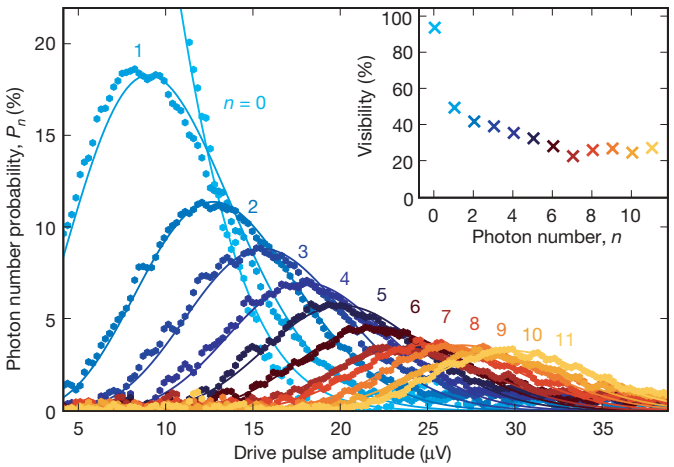

Figure 4 | Population analysis of coherent states. The points represent the amplitudes of the Fourier transforms in Fig. 3d, obtained along the dashed vertical lines, corrected for the measurement visibility of 80% and transformed into photon number probabilities using equations (2) and (3). The solid lines are the photon number probabilities predicted by the Poisson distribution in equation (4). To fit the measured distribution, the solid lines have been scaled by an individual visibility factor for each photon number (inset). The visibility for $n = 0$ is close to 100%; the visibilities for $n > 0$ are lower because decoherence during the measurement lowers the corresponding Fourier amplitudes.

Received 19 March; accepted 23 May 2008.

1. Cohen-Tannoudji, C., Diu, B. & Laloë, F. *Quantum Mechanics* Vol. 1, Ch. 4 5 (Wiley, New York, 2006).
2. Haroche, S. & Raimond, J.-M. *Exploring the Quantum — Atoms, Cavities and Photons* Ch. 3 (Oxford Univ. Press, Oxford, UK, 2006).
3. Meekhof, D. M., Monroe, C., King, B. E., Itano, W. M. & Wineland, D. J. Generation of nonclassical motional states of a trapped atom. *Phys. Rev. Lett.* **76,** 1796–1799 (1996).
4. Cirac, J. I., Blatt, R., Parkins, A. S. & Zoller, P. Preparation of Fock states by observation of quantum jumps in an ion trap. *Phys. Rev. Lett.* **70,** 762–765 (1993).
5. Varcoe, B. T. H., Brattke, S., Weidinger, M. & Walther, H. Preparing pure photon number states of the radiation field. *Nature* **403,** 743–746 (2000).
6. Bertet, P. *et al.* Generating and probing a two-photon Fock state with a single atom in a cavity. *Phys. Rev. Lett.* **88,** 143601 (2002).
7. Waks, E., Dimanti, E. & Yamamoto, Y. Generation of photon number states. *N. J. Phys.* **8,** 4 (2006).
8. Devoret, M. & Martinis, J. M. Implementing qubits with superconducting integrated circuits. *Quantum Inf. Process.* **3,** 163–203 (2004).
9. Guerlin, C. *et al.* Progressive field-state collapse and quantum non-demolition photon counting. *Nature* **448,** 889–893 (2007).
10. Wallraff, A. *et al.* Strong coupling of a single photon to a superconducting qubit using circuit quantum electrodynamics. *Nature* **431,** 162–167 (2004).
11. Johansson, J. *et al.* Vacuum Rabi oscillations in a macroscopic superconducting qubit LC oscillator system. *Phys. Rev. Lett.* **96,** 127006 (2006).
12. Houck, A. A. *et al.* Generating single microwave photons in a circuit. *Nature* **449,** 328–331 (2007).
13. Sillanpää, M. A., Park, J. I. & Simmonds, R. W. Coherent quantum state storage and transfer between two phase qubits via a resonant cavity. *Nature* **449,** 438–442 (2007).
14. Majer, J. *et al.* Coupling superconducting qubits via a cavity bus. *Nature* **449,** 443–447 (2007).
15. Schuster, D. I. *et al.* Resolving photon number states in a superconducting circuit. *Nature* **445,** 515–518 (2007).
16. Astafiev, O. *et al.* Single artificial-atom lasing. *Nature* **449,** 588–590 (2007).
17. Liu, Y.-X., Wei, L. F. & Nori, F. Generation of nonclassical photon states using a superconducting qubit in a microcavity. *Europhys. Lett.* **67,** 941–947 (2004).
18. Brune, M. *et al.* Quantum Rabi oscillation: A direct test of field quantization in a cavity. *Phys. Rev. Lett.* **76,** 1800–1803 (1996).
19. Steffen, M. *et al.* State tomography of capacitively shunted phase qubits with high fidelity. *Phys. Rev. Lett.* **97,** 050502 (2006).
20. Neeley, M. *et al.* Transformed dissipation in superconducting quantum circuits. *Phys. Rev. B* **77,** 180508(R) (2008).
21. O'Connell, A. D. *et al.* Microwave dielectric loss at single photon energies and millikelvin temperatures. *Appl. Phys. Lett.* **92,** 112903 (2008).
22. Neeley, M. *et al.* Process tomography of quantum memory in a Josephson phase qubit coupled to a two-level state. *Nature Phys.* advance online publication doi:10.1038/nphys972 (27 April 2008).
23. Devoret, M. H., Esteve, D., Martinis, J. M. & Urbina, C. Effect of an adjustable admittance on the macroscopic energy levels of a current biased Josephson junction. *Phys. Scr.* **T25,** 118–121 (1989).
24. Devoret, M. H. *et al.* in *Quantum Tunnelling in Condensed Media* (eds Kagan, Y. & Leggett, A. J.) Ch. 6 337–338 (Elsevier, Amsterdam, 1992).
25. Jaynes, E. & Cummings, F. Comparison of quantum and semiclassical radiation theories with application to the beam maser. *Proc. IEEE* **51,** 89–109 (1963).
26. Lucero, E. *et al.* High-fidelity gates in a Josephson qubit. *Phys. Rev. Lett.* (in the press); preprint at ⟨http://arxiv.org/abs/0802.0903⟩ (2008).
27. Lu, N. Effects of dissipation on photon statistics and the lifetime of a pure number state. *Phys. Rev. A* **40,** 1707–1708 (1989).
28. Faist, A., Geneux, E., Meystre, P. & Quattropani, P. Coherent radiation in interaction with two-level system. *Helv. Phys. Acta* **45,** 956–959 (1972).
29. Eberly, J. H., Narozhny, N. B. & Sanchez-Mondragon, J. J. Periodic spontaneous collapse and revival in a simple quantum model. *Phys. Rev. Lett.* **44,** 1323–1326 (1980).
30. Leibfried, D. *et al.* Experimental determination of the motional quantum state of a trapped atom. *Phys. Rev. Lett.* **77,** 4281–4285 (1996).

Acknowledgements We thank M. Geller for theoretical input. Devices were made at the UCSB Nanofabrication Facility, a part of the NSF-funded National Nanotechnology Infrastructure Network. This work was supported by IARDA under grant W911NF-04-1-0204 and by the NSF under grants CCF-0507227 and DMR-0605818.

Author Information Reprints and permissions information is available at www.nature.com/reprints. Correspondence and requests for materials should be addressed to A.N.C. (cleland@physics.ucsb.edu).